Crystal Structure of a Helix Layered Silicate Containing Tetramethylammonium Ions in Sodalite-Like Cages

T. Ikeda,*,† Y. Akiyama,‡ F. Izumi,† Y. Kiyozumi,§ F. Mizukami,§ and T. Kodaira§

National Institute for Research in Inorganic Materials, 1-1 Namiki, Tsukuba, Ibaraki 305-0044, Japan, Amersham Pharmacia Biotech K. K., Sanken Building, 3-25-1 Hyakunin-cho, Shinjuku-ku, Tokyo 169-0073, Japan, and National Institute of Materials and Chemical Research, 1-1 Higashi, Tsukuba, Ibaraki 305-8565, Japan

Received September 12, 2000. Revised Manuscript Received January 3, 2001

The crystal structure of a helix layered silicate (HLS), $[(CH_3)_4N]_2Na_2[Si_{10}O_{20}(OH)_4]\cdot 5.53H_2O$, with tetramethylammonium (TMA) ions as templates was determined by ab initio structure analysis with X-ray powder diffraction data. The HLS is orthorhombic with space group *Amm*2 and lattice parameters of $a = 22.8641(2)$ Å, $b = 12.5388(2)$ Å, and $c = 12.4648(2)$ Å. A $Q^3-Q^4-Q^3$ silicon network with an amount-of-substance ratio of Si/O = 1:2.4 exhibits cup-shaped cage topology with four- and six-membered rings. Such a cage is similar to a sodalite cage divided into two pieces. ^{29}Si MAS NMR showed the silicate layer to have Q^3- and Q^4-types of Si atoms with a Q^3/Q^4 ratio of ca. 4.0, which is consistent with our structural model. The framework is distorted, with Si−O bond lengths varying widely. TMA ions are incorporated into the cup-shaped cage. Na^+ ions and H_2O molecules are also located between two silicate layers, with interlayer distances varying alternately. Disordering of TMA ions, Na^+ ions, and H_2O molecules was clearly visualized in electron-density maps obtained by combining a maximum-entropy method and whole-pattern fitting. H_2O molecules surround Na^+ ions and form hydrogen bonds with O atoms in silanol groups in the silicate layers, by which the lattice instability due to the distorted framework is compensated. The present compound is regarded as a metastable phase, as would be expected for precursors to new types of microporous materials with silicate frameworks such as the sodalite cage.

1. Introduction

Novel microporous materials incorporating various organic templates have been widely investigated. High-silica layered silicates are also of considerable interest because they are promising candidates for precursors to new microporous and mesoporous materials. A RUB series reported by Gies et al.[1−4] since 1990 has particularly received much attention because of its unique structural features such as cage-like frameworks of silicate layers, $[Na(H_2O)_6]^+$ octahedra, and quarternary ammonium ions as templates. The sizes of the template ions match those of small cup-shaped cages in these precursors, which is essential to construction of the framework structures. Other cage-containing and microporous materials such as RUB-15,[1] RUB-10,[3] Nu-1,[5] ZSM-5,[6] offretite,[7] and sodalite[8,9] also incorporate quarternary ammonium ions.[10,11] In these materials, alkyl groups in the template ions rotate freely around C−N bonds. Such rotational disorder leads to apparent high symmetry, with tetrahedral configurations of the alkyl groups around N atoms.

Crystal structures of layered silicates are complicated. Generally, they have poor crystallinity and cannot be grown into single crystals. They also include Si atoms of Q^3 and Q^4 types as observed in their NMR spectra, in contrast with the Si atoms of only the Q^4 type in zeolites and other microporous materials. Their framework structures are, therefore, difficult to determine by X-ray diffraction, with the result that crystal structures of many interesting layered silicates, e.g., makatite and magadiite, remain unknown.

The crystal structure of a layered silicate, kanemite, was analyzed by Gies et al.[4,12] Its structure has a network composed of only Q^3-type Si atoms and $[Na(H_2O)_6]^+$ octahedra sandwiched between two silicate

* Corresponding author: T. Ikeda, National Institute for Research in Inorganic Materials, 1-1 Namiki, Tsukuba, Ibaraki 305-0044, Japan. E-mail: ikeda@nirim.go.jp. Fax: +81-298-52-7449.
† National Institute for Research in Inorganic Materials.
‡ Amersham Pharmacia Biotech K. K.
§ National Institute of Materials and Chemical Research.

(1) Oberhagemann, U.; Bayat, P.; Marler, B.; Gies, H.; Rius, J. *Angew. Chem., Int. Ed. Engl.* **1996**, *35*, 2869.
(2) Vortmann, S.; Rius, J.; Siegmann, S. J.; Gies, H. *J. Phys. Chem. B* **1997**, *101*, 1292.
(3) Gies, H.; Rius, J. *Z. Kristallogr.* **1995**, *210*, 475.
(4) Gies, H.; Marler, B.; Vortmann, S.; Oberhagemann, U.; Bayat, P.; Krink, K.; Rius, J.; Wolf, I.; Fyfe, C. *Microporous Mesoporous Mater.* **1998**, *21*, 183.
(5) Bhaumik, A.; Tatsumi, T. *Microporous Mesoporous Mater.* **2000**, *34*, 1.
(6) Van Koningsveld, H.; Van Bekkum, H.; Jansen, J. C. *Acta Crystallogr.* **1987**, *B43*, 127.
(7) Newsam, J. M.; Vaughan, D. E. W. *Stud. Surf. Sci. Catal.* **1986**, *28*, 457.
(8) Hong, S. B.; Camblor, M. A.; Davis, M. E. *J. Am. Chem. Soc.* **1997**, *119*, 761.
(9) Baerlocher, C.; Meier, W. M. *Helv. Chim. Acta.* **1969**, *52*, 1853.
(10) Testa, F.; Crea, F.; Nastro, A.; Aiello, R.; Mostowicz, R.; Nagy, J. B. *Zeolites* **1991**, 11, 633.
(11) Aiello, R.; Cref, F.; Nastro, A.; Pellegrino, C. *Zeolites* **1987**, *7*, 549.
(12) Vortmann, S.; Rius, J.; Marler. B.; Gies, H. *Eur. J. Mater.* **1999**, *11*, 125.

10.1021/cm000736v CCC: $20.00
Published on Web 03/13/2001

layers. Such a structure containing Q^3-type Si atoms seems to be unstable from the viewpoint of crystal chemistry. Kanemite serves as a precursor to silicalite-1 (MFI), ZSM-11 (MEL), mesoporous MCM-41, and other microporous materials.[13−15] No mechanisms of structural changes during the preparation of these materials have yet been clarified. However, we can recognize structural similarities among kanemite, MFI, and MEL, considering that a group of Q^3-type Si atoms in kanemite can be changed into a five-membered ring by addition of Si atoms.

Akiyama et al.[16,17] have recently synthesized a new helix layered silicate (HLS) hydrothermally. The name of the HLS originates from its characteristic morphology of platy microcrystals stacked helically. Tetramethylammonium (TMA), Na^+ and OH^- ions, and H_2O molecules are incorporated into the HLS. TG-DTA revealed its thermal stability to be low. In fact, the HLS is converted into some intermediate phases that are structurally similar to the HLS. We expect the HLS to be a promising precursor to new high-silica microporous materials. Detailed crystallographic data of the HLS are indispensable for an understanding of its physical and chemical properties.

In this work, we have determined the crystal structure of the HLS from X-ray powder diffraction (XRD) data, using a direct method,[18,19] the Rietveld method and whole-pattern fitting based on a maximum-entropy method (MEM).[20−22] MEM is a versatile approach to the estimation of a model from a limited amount of information by maximizing information entropy under constraints consistent with observed physical quantities. In recent years, Sakata et al.[23,24] have applied it actively to the determination of electron densities using powder diffraction data. MEM infers electron densities in such a way that they provide the maximum variance of structure factors within errors in observed structure factors, F_o. Imaging electron densities by MEM also makes it possible to find unknown and/or disordered sites much more definitely than that by Fourier/D synthesis.[25−27] Takata et al.[28] combined MEM and the Rietveld method to analyze crystal structures of various compounds, including a series of metallofullerenes. Our original technology of MEM-based whole-pattern fitting is superior to the MEM/Rietveld method in the point that the bias toward the structural model can be effectively reduced by iterative procedures named REMEDY cycles.[20,22]

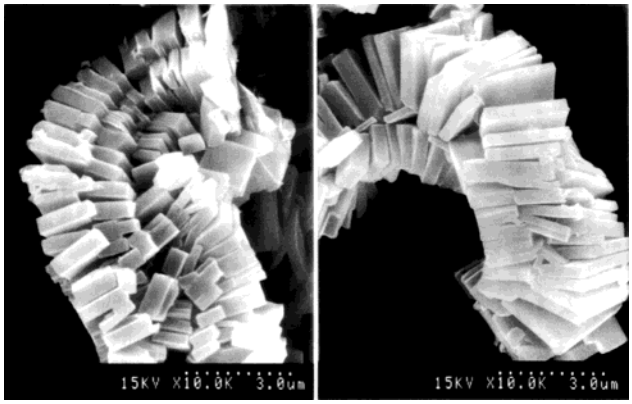

Figure 1. Scanning electron micrographs of the HLS.

Our structure analysis of the HLS has revealed a layered framework with cup-shaped cages whose topology is similar to that of a sodalite cage. In addition, whole-pattern fitting based on MEM has enabled us to visualize disordered arrangements of TMA ions in the cup-shaped cages and Na^+ ions and H_2O molecules between two silicate layers. We will discuss detailed structural properties of the HLS in terms of its crystal data and electron densities determined by the Rietveld and MEM analyses, respectively.

2. Experimental Section

2.1. Sample Preparation. A sample of the HLS was prepared hydrothermally from SiO_2 (Cab-O-sil M5), 1,4-dioxane, $[(CH_3)_4N]OH$, NaOH, and H_2O. The mixture was heated in a Teflon-lined autoclave at 150 °C for 5 days. The resultant powder was separated from the solution by filtration, washed with acetone, and dried at 70 °C for a few hours. Detailed synthetic procedures were reported before.[16] Observations by scanning electron microscopy (SEM) with a Hitachi S-800 microscope showed the sample to be composed of helical stacks of microcrystals with a length of ca. 3 μm along the plate (Figure 1).

2.2. Quantitative Analysis. The Si and Na contents in the HLS analyzed by ICP emission spectrometry were 71.1 wt % as SiO_x and 4.9 wt %, respectively. We found the linkages of the TMA ion to be maintained in the HLS on the basis of an FT Raman spectrum measured on a Bruker RFS-100 instrument equipped with an FRA-106 sample stage (Figure 2). The TMA content determined with a CHN elemental analyzer was 13.3 wt %. The water content was estimated at ca. 10.7 wt % by TG with a MAC Science TG-DTA 2100 instrument in dried air. These contents depended on conditions such as humidity and temperature. TG-DTA revealed that H_2O was released up to 165 °C and that TMA ions decomposed near 385 °C (Figure 3).

Figure 4 shows a solid-state ^{29}Si MAS NMR spectrum measured with a spinning frequency of 4 kHz, a 30° pulse length of 1.5 μs, and a cycle delay time of 180 s on a Chemagnetics CMX-300 spectrometer operated at 59.65 MHz. Spectra obtained by ca. 280 scans were accumulated, and ^{29}Si chemical shifts were calibrated with a standard sample of hexamethyldimethylsiloxane. A solid-state ^{13}C CP-MAS NMR spectrum was also measured with a spinning frequency of 4 kHz, a 90° pulse length of 4.7 μs, and a cycle delay time of 10 s on a Bruker AMX-500 spectrometer operated at 125.78 MHz (Figure 5).

2.3. XRD Measurement. XRD data of the HLS were collected at room temperature on a MAC Science MXP-18VTZ

(13) Salou, M.; Kiyozumi, Y.; Nair, P.; Mizukami, F.; Maeda, K.; Niwa, S. *J. Mater. Chem.* **1998**, *8*, 2125.
(14) Shimizu, S.; Kiyozumi, Y.; Mizukami, F. *Chem. Lett.* **1996**, 403.
(15) Chen, C.-Y.; Xian, S.-Q.; Davis, M. E. *Microporous Mater.* **1995**, *4*, 1.
(16) Akiyama, Y.; Mizukami, F.; Kiyozumi, Y.; Maeda, K.; Izutsu, H.; Sakaguchi, K. *Angew. Chem., Int. Ed. Engl.* **1999**, *10*, 1420.
(17) Akiyama, Y.; Mizukami, F.; Kiyozumi, Y.; Ikeda, T., manuscript to be submitted.
(18) Harris, K. D. M.; Tremayne, M. *Chem. Mater.* **1996**, *8*, 2554.
(19) Massatotti, V.; Capsoni, D.; Bini, M.; Altomare, A.; Moliterni, A. A. G. *Z. Kristallogr.* **1999**, *214*, 205.
(20) Izumi, F.; Kumazawa, S.; Ikeda, T.; Ida, T. In *Powder Diffraction*; Sen Gupta, S. P., Ed.; Allied Publishers: New Delhi, India, 1998; pp 24−36.
(21) Izumi, F.; Ikeda, T. *Mater. Sci. Forum* **2000**, *321−324*, 1983.
(22) Izumi, F.; Kumazawa, S.; Ikeda, T. Hu, W.-Z.; Yamamoto, A.; Oikawa, K. *Mater. Sci. Forum*, in press.
(23) Sakata, M.; Sato, M. *Acta Crystallogr.* **1990**, *A46*, 263.
(24) Takata, M.; Sakata, M. *Acta Crystallogr.* **1996**, *A52*, 287.
(25) Papoular, R. J.; Cox, D. E. *Europhys. Lett.* **1995**, *32*, 337.
(26) Ikeda, T.; Izumi, F.; Kodaira, T.; Kamiyama, T. *Chem. Mater.* **1998**, *10*, 3996.
(27) Knorr, K.; Madler, F.; Papoular, R. J. *Microporous Mesoporous Mater.* **1998**, *21*, 353.
(28) Takata, M.; Umeda, B.; Nishibori, E.; Sakata, M.; Saito, Y.; Ohno, M.; Shinohara, H. *Nature* **1995**, *377*, 46.

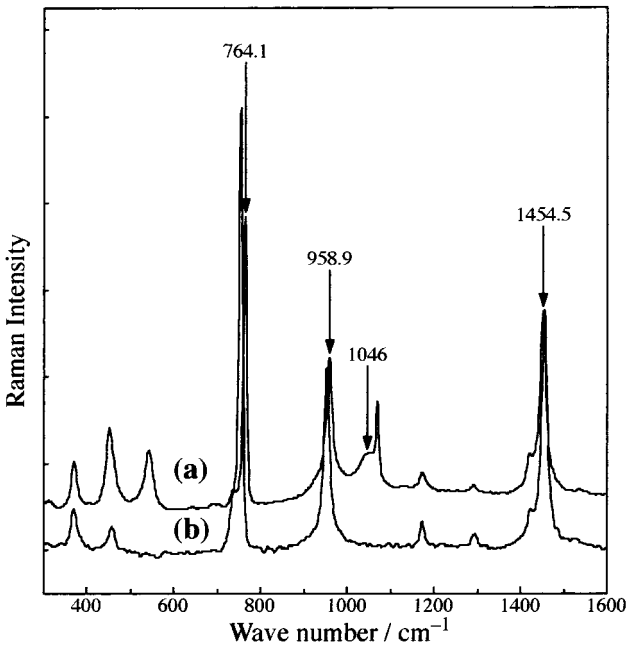

Figure 2. Raman spectra of (a) TMA ions incorporated into the HLS and (b) TMA ions in an aqueous solution.

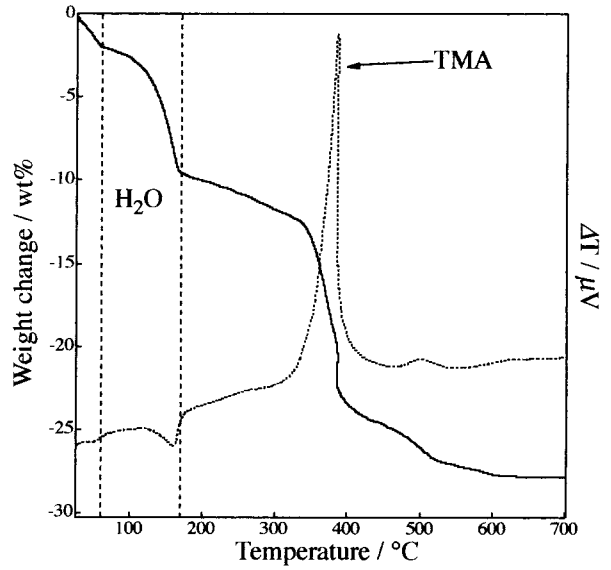

Figure 3. TG-DTA curves of the HLS. The region encompassed by the TG curve (solid line) indicates the release of H_2O. The exothermic peak near 385 °C in the DTA curve (broken line) corresponds to decomposition of TMA ions.

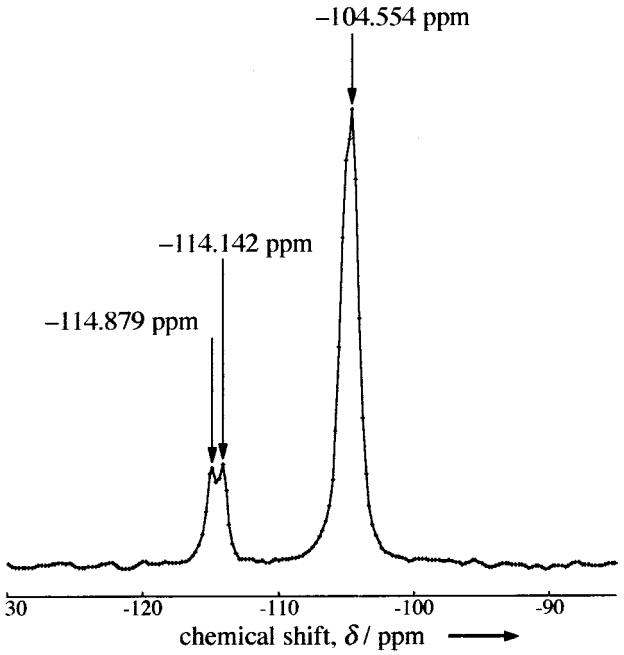

Figure 4. ^{29}Si MAS NMR spectrum of the HLS. One Q^3 and two Q^4 peaks have an integrated-intensity ratio, Q^3/Q^4, of ca. 4.1.

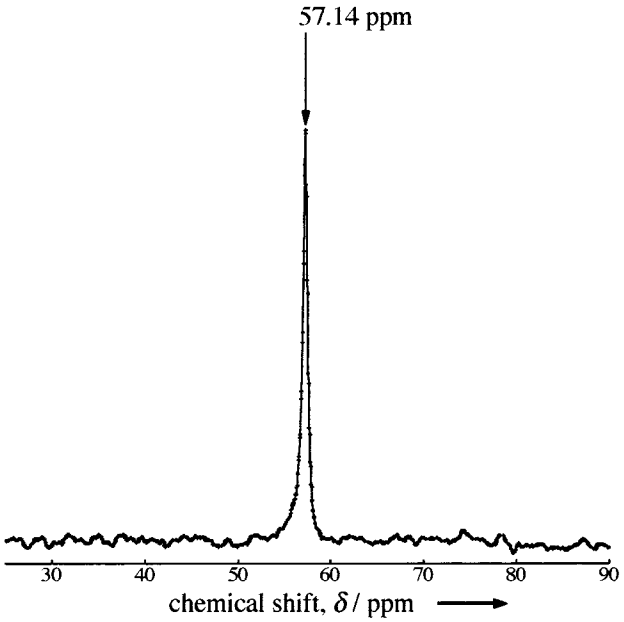

Figure 5. ^{13}C CP-MAS NMR spectrum of the HLS.

powder diffractometer with a vertical θ:θ geometry. To suppress axial divergence and make diffraction profiles in the low-angle region as symmetric as possible, its goniometer was equipped with a pair of long Soller slits to decrease the angular aperture to 1°. The sample was packed in a glass holder as thick as 5 mm to keep the absorption factor constant regardless of 2θ. The conditions of the XRD experiment were as follows: Cu Kα radiation; output = 50 kV and 300 mA using a rotating anode; step width = 0.01° for 6.5° < 2θ < 17.3°, 0.016° for 17.3° < 2θ < 35.0°, and 0.022° for 35.0° < 2θ < 103.0°; counting time per step = 100 s. Other experimental conditions are included in Table 1. The goniometer was provided with variable-width divergence and scattering slits to improve counting statistics in the high-2θ region by fixing the irradiation width at 20 mm and to suppress the background level in the low-2θ region, respectively. Throughout subsequent whole-pattern decomposition and structure refinements, we included a factor to correct for the effect of the constant irradiation width on the calculated intensity (model function).

3. Structure Analysis

3.1. Derivation of a Structural Model. The crystallinity of the sample seemed to be sufficient for its structure to be determined by XRD. No effects of preferred orientation and coarse crystals on integrated intensities were observed, as evidenced by the smooth curve measured for more than 20 reflections with an ω-scan technique (Figure 6).[29]

Indexing of reflections with TREOR90[30] built into PowderX[31] gave an orthorhombic unit cell of a = 22.874-

(29) Yukino, K.; Uno, R. *Jpn. J. Appl. Phys.* **1986**, *25*, 661.
(30) Werner, P.-E. *Z. Kristallogr.* **1964**, *120*, 375.

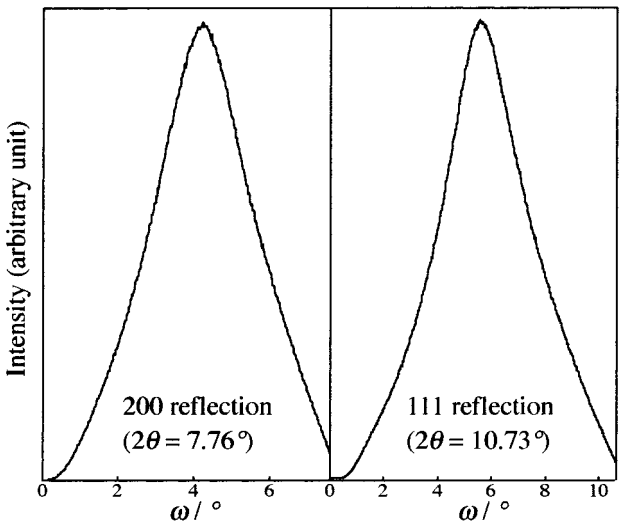

Figure 6. Profiles of the ω scan for the 200 (left) and 111 (right) reflections.

Table 1. Conditions of the XRD Experiment and Crystallographic Data for HLS

compound name	Helix Layered Silicate (HLS)
chemical formula	$[(CH_3)_4N]_2Na_2[Si_{10}O_{20}(OH)_4]\cdot 5.53H_2O$
F_W	3849.17
space group	*Amm*2 (no. 38)
Z	4
a (Å)	22.8641(2)
b (Å)	12.5388(2)
c (Å)	12.4648(2)
unit-cell volume (Å^3)	3573.94(8)
wavelength λ (Å)	1.5418 (Cu Kα)
2θ range (°)	6.5−103
step size (2θ) (°)	0.01−0.022
profile range in fwhm	14
number of observations	5152
number of contributing reflections	2336
number of structural parameters	109
number of geometric constraints	98
R_F	0.0091
R_{wp}	0.0585
R_e	0.0551

(7) Å, b = 12.537(5) Å, and c = 12.476(3) Å with the acceptable figures of merit F_{30} = 24 (0.010845, 119) and M_{20} = 43. Reflection conditions derived from the indexed reflections were $h + k = 2n$ for hkl, $k = 2n$ for $0kl$, $h = 2n$ for $h0l$, $h + k = 2n$ for $hk0$, $h = 2n$ for $h00$, and $k = 2n$ for $0k0$, affording space group *Cmmm* (no. 65) on the assumption that the HLS has a centrosymmetric space group. Some weak reflections that are probably due to another high-silica phase were excluded in subsequent structure analysis.

The observed integrated intensities, $|F_o|^2$, of 1316 reflections in the region of $d > 1.2$ Å were extracted by the Le Bail method[32] with a versatile pattern-fitting system RIETAN-2000.[20−22,33] A split pseudo-Voigt function of Toraya[34] was used as the profile function. Partial profile relaxation with a modified split pseudo-Voigt function[20,21] was applied to 14 reflections in the region of 2θ lower than 26°, which significantly improved fits between the observed and calculated profiles. A similar profile-fitting technique was utilized in Rietveld refinement and MEM-based whole-pattern fitting, which will be described later. R factors were R_{wp} = 8.15% (R_e = 7.20%) and R_p = 5.18%. The use of the medium-resolution data in the above d region was effective in reducing structural ambiguity arising from the inclusion of high-angle reflections whose $|F_o|^2$ values could not be determined with sufficient accuracy.[35−37]

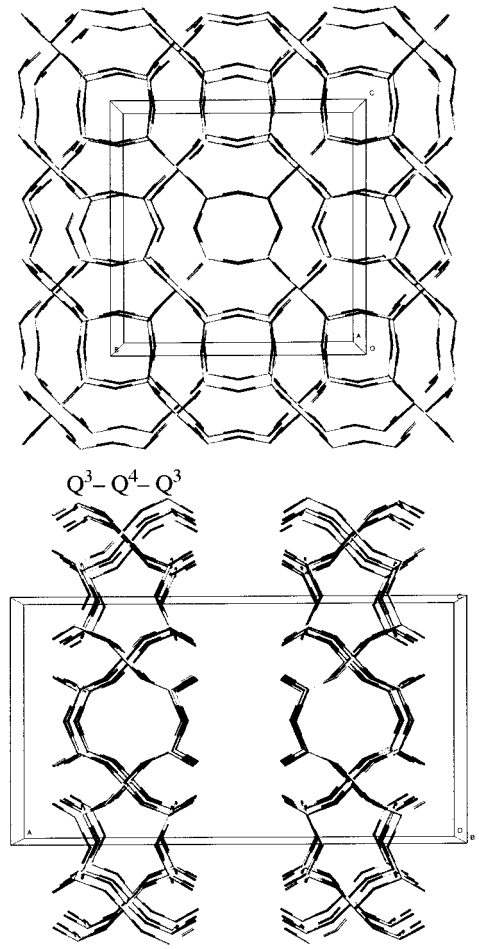

Figure 7. Perspective view of the framework for the HLS along the [100] (upper) and [010] (lower) directions. Dark and light gray sticks indicate bonds of Si and O atoms, respectively.

The framework of the HLS could unequivocally be derived from the $|F_o|^2$ values by a direct method using SIRPOW97 in EXPO.[38] Figure 7 illustrates that the HLS framework contains Q^3 and Q^4 types of Si atoms. Because TMA ions, Na^+ ions, and H_2O molecules could not be located at this stage, we tried to learn their positions by the MEM/Rietveld method.[28]

A starting structural model included 10 sites located by the direct method: three Si and seven O sites. In a Rietveld refinement with this model, we imposed con-

(31) Dong, C. *J. Appl. Crystallogr.* **1999**, *32*, 838.
(32) Le Bail, A.; Duroy, H.; Fourquet, J. L. *Mater. Res. Bull.* **1988**, *23*, 447.
(33) Izumi, F. In *The Rietveld Method*; Young, R. A., Ed.; Oxford University Press: Oxford, U.K., 1995; Chapter 13.
(34) Toraya, H. *J. Appl. Crystallogr.* **1990**, *23*, 485.
(35) Rius, J. *Acta Crystallogr.* **1993**, *A49*, 406.
(36) Rius, J.; Miravitlles, C.; Amigo, J. M.; Reventos, M. M. *Acta Crystallogr.* **1995**, *A51*, 268.
(37) Rius, J.; Miravitlles, C.; Sane, J.; Gies, H.; Marler, B.; Oberhagemann, U. *Acta Crystallogr.* **1995**, *A51*, 840.
(38) Altomare, A.; Burla, M. C.; Camalli, M.; Carrozzini, B.; Cascarano, G. L.; Giacovazzo, C.; Guagliardi, A.; Moliterni, A. G. G.; Polidori, G.; Rizzi, R. *J. Appl. Crystallogr.* **1999**, *32*, 339.

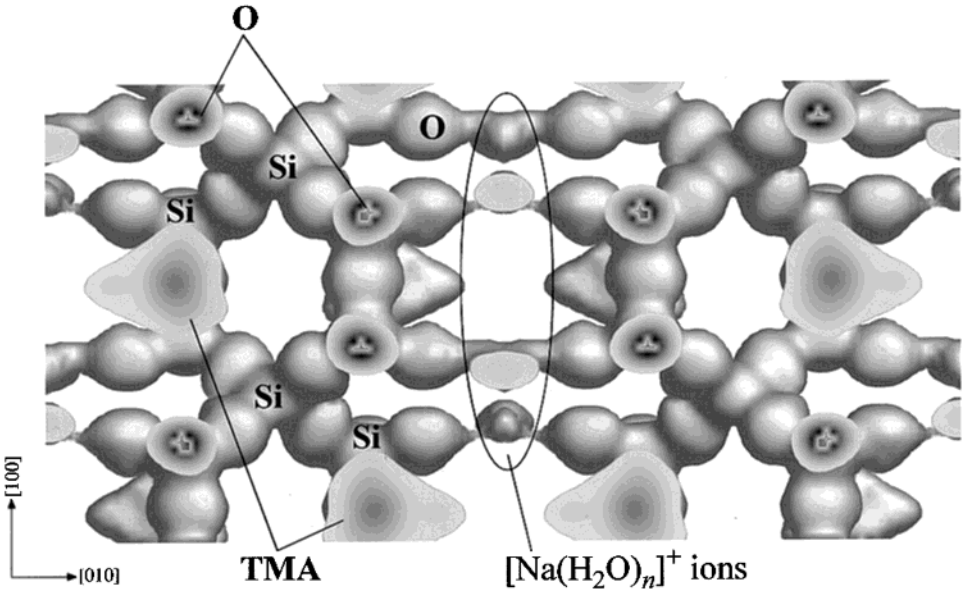

Figure 8. Preliminary electron-density image viewed along the [010] direction. Approximate locations of TMA ions, Na^+ ions, and H_2O molecules are visualized. The equi-density level was set at 0.4 e/Å^3.

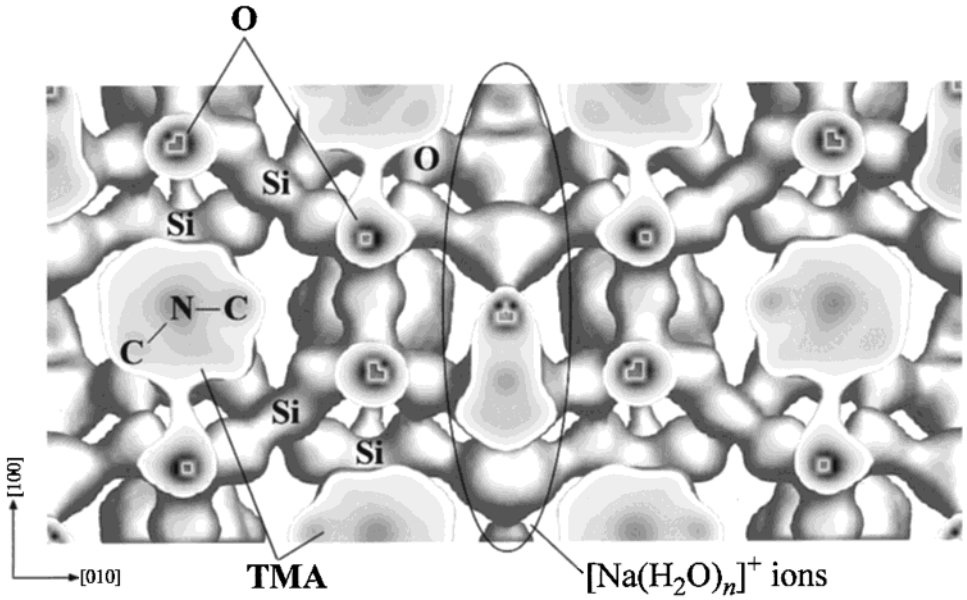

Figure 9. Electron-density image resulting from the revised structural model. TMA ions are found to exhibit rotational disorder. Na^+ ions and H_2O molecules connect two silicates layers. The equi-density level was set at 0.4 e/Å^3.

straints on all of the Si−O bond lengths l(Si−O) such that l(Si−O) = 1.62 ± 0.05 Å. Then, F_o values and their calculated standard deviations, σ, of 328 reflections in the region d > 1.2 Å were estimated from the observed intensities and calculated profiles of the reflections according to the procedures of Rietveld[39] and Kumazawa,[40] respectively. They were analyzed by MEM with MEED[41] at a space resolution of 128 × 64 × 64 pixels per unit cell to give R factors of R_F = 20.0% and wR_F = 18.5%. These R factors are defined as

$$R_F = \sqrt{\frac{\sum|F_o - F_{MEM}|}{\sum|F_o|}}$$

and

$$wR_F = \frac{\sum|F_o - F_{MEM}|/\sigma^2}{\sum|F_o|/\sigma^2}$$

where F_{MEM} is the structure factor estimated by the MEM analysis and the summation is carried out over all of the reflections analyzed by MEM.[40]

The above MEM analysis yielded electron-density images that indicated the approximate positions of TMA ions and atoms sandwiched between two silicate layers (Figure 8). Highly covalent Si−O bonds in the framework are manifest in this figure. The structural model was then revised to include the contributions of these bonds to the observed intensities. A virtual chemical

(39) Rietveld, H. M. *J. Appl. Crystallogr.* **1969**, *2*, 65.

(40) Kumazawa, S. D. Eng. Thesis, Nagoya University, Nagoya, 1995.

(41) Kumazawa, S.; Kubota, Y.; Takata, M.; Sakata, M.; Ishibashi, Y. *J. Appl. Crystallogr.* **1993**, *26*, 453.

Table 2. Structure Parameters of the HLS at Room Temperature ($Z = 4$)'

atom	site		g	x	y	z	B (Å^2)
Si1	8f	1		0.1514(3)	−0.1305(5)	−0.1855(8)	1.27(2)
Si1b	8f	1		0.6506(3)	−0.1221(5)	0.3100(11)	=B(Si1)
Si2	8f	1		0.1521(4)	0.1217(5)	0.0651(8)	=B(Si1)
Si2b	8f	1		0.6527(5)	0.1254(6)	0.5603(9)	=B(Si1)
Si3	8f	1		0.2498(5)	0.2514(8)	0.1844(11)	=B(Si1)
O1	4c	1		0.1549(8)	0	0.082(2)	3.29(8)
O2	8f	1		0.1542(5)	0.1511(10)	−0.0742(14)	=B(O1)
O3	4c	1		0.1521(7)	0	−0.2101(13)	=B(O1)
O4	8f	1		0.2108(8)	0.1769(14)	0.1206(10)	=B(O1)
O5	8f	1		0.2099(7)	−0.1820(11)	−0.2402(13)	=B(O1)
O6	8f	1		0.1011(7)	−0.1815(12)	−0.2330(11)	2.02(12)
O7	8f	1		0.0994(7)	0.1698(12)	0.1168(11)	=B(O6)
O1b	4c	1		0.6501(8)	0	0.5810(14)	=B(O1)
O2b	8f	1		0.6511(5)	0.1456(10)	0.4265(14)	=B(O1)
O3b	4c	1		0.6567(8)	0	0.290(2)	=B(O1)
O4b	8f	1		0.7130(8)	0.1725(14)	0.6047(13)	=B(O1)
O5b	8f	1		0.7083(8)	−0.1797(11)	0.2583(14)	=B(O1)
O6b	8f	1		0.5869(6)	−0.1716(11)	0.2565(14)	=B(O6)
O7b	8f	1		0.6024(8)	0.1823(10)	0.6148(14)	=B(O6)
Na1	4d	1		0	0.2228(14)	0.044(2)	6.4(4)
Na2	8f	1/2		0.5780(8)	0.0674(14)	0.045(2)	=B(Na1)
C1	4c	1		0.336(2)	1/2	0.323(2)	3.0(3)
C2	4c	1/2		0.290(2)	1/2	0.491(3)	=B(C1)
C3	8f	1/2		0.3837(13)	0.400(2)	0.452(3)	=B(C1)
C4	4c	1/2		0.4160(14)	1/2	0.436(4)	=B(C1)
C5	8f	1/2		0.324(2)	0.599(2)	0.478(3)	=B(C1)
N1	4c	1		0.3486(9)	1/2	0.424(2)	=B(C1)
C1b	4c	1		0.8070(12)	1/2	0.881(2)	=B(C1)
C2b	4c	1/2		0.8476(14)	1/2	0.052(3)	=B(C1)
C3b	8f	1/2		0.8890(11)	0.424(2)	0.931(4)	=B(C1)
C4b	4c	1/2		0.911(2)	1/2	0.888(4)	=B(C1)
C5b	8f	1/2		0.8600(11)	0.589(3)	0.0149(14)	=B(C1)
N2	4c	1		0.8613(8)	1/2	−0.0490(12)	=B(C1)
WO1	4d		0.6917(2)	0	0.361(2)	0.114(2)	2.6(3)
WO2	4d		=g(WO1)	0	0.052(2)	0.214(2)	=B(WO1)
WO3	4d		=g(WO1)	0	−0.398(3)	0.239(3)	=B(WO1)
WO4	4d		=g(WO1)	0	0.0862(13)	−0.095(2)	=B(WO1)
WO1b	4e		=g(WO1)	1/2	0.171(2)	0.454(3)	=B(WO1)
WO2b	4e		=g(WO1)	1/2	0.060(2)	0.695(2)	=B(WO1)
WO3b	4e		=g(WO1)	1/2	−0.389(2)	0.739(3)	=B(WO1)
WO4b	4e		=g(WO1)	1/2	0.161(2)	0.583(2)	=B(WO1)

species whose atomic scattering factor is equal to the sum of those for 4 C, 12 H, and 1 N atoms was positioned to take the place of each TMA ion. Electron-density images obtained by combining MEM and Rietveld analyses unequivocally revealed that the TMA and Na^+ ions and H_2O molecules were highly disordered, as can be appreciated from Figure 9. Rietveld and MEM analyses were alternately repeated in this manner until their results became consistent with each other. MEM analysis at this stage afforded R factors, $R_F = 6.5\%$ and $wR_F = 5.5\%$, that were much lower than those at the preceding stage.

The ^{29}Si MAS NMR spectrum showed one Q^3 and two Q^4 peaks with an integrated-intensity ratio of $Q^3/Q^4 \approx 4.10$ (Figure 4). This ratio is in fair agreement with the value of 4 calculated from the framework topology. The presence of the two types of the Q^4-type Si atoms indicates that the local chemical environments of the Q^3-type Si atoms neighboring each Q^4 site differ slightly and that the SiO_4 tetrahedra are somewhat distorted. This experimental fact can be ascribed to sample inhomogeneity with respect to the amounts of Na^+ ions and H_2O molecules, the orientations of the TMA ions, and so on. However, space group *Cmmm* affords only two Q^3 sites and one Q^4 site. Because the Q^3 site should occupy a position with a higher degree of freedom, the HLS must have a symmetry lower than *Cmmm*. On the other hand, isotropic atomic displacement parameters, B, of the Q^4-type Si atoms converged at reasonable

Table 3. Selected Geometric Parameters for the HLS[a]

			l (Å)				l (Å)
Si1^{i}	−	O2	1.420(20)	N1	−	C5	1.52(2)
Si1	−	O3	1.665(6)	N2	−	C1b	1.51(2)
Si1	−	O5	1.630(20)	N2	−	C2b	1.31(3)
Si1	−	O6	1.445(14)	N2	−	C3b	1.19(2)
Si2	−	O1	1.543(7)	N2	−	C4b	1.39(3)
Si2	−	O2	1.770(20)	N2	−	C5b	1.37(2)
Si2	−	O4	1.660(20)	Na1	−	O7	2.54(2)
Si2	−	O7	1.494(14)	Na1	−	WO1	1.94(2)
Si1b	−	O2b^{ii}	1.480(20)	Na1	−	WO4	2.43(3)
Si1b	−	O3b	1.559(6)	Na2	−	O6b^{i}	2.95(2)
Si1b	−	O5b	1.630(20)	Na2	−	N1^{iii}	2.40(3)
Si1b	−	O6b	1.717(14)	WO1	−	WO3	1.64(5)
Si2b	−	O1b	1.595(7)	WO2	−	O7	2.97(2)
Si2b	−	O2b	1.682(14)	WO3	−	WO4^{v}	2.07(4)
Si2b	−	O4b	1.600(20)	WO3	−	WO3^{iv}	2.07(4)
Si2b	−	O7b	1.518(14)	WO3	−	O6^{vi}	2.54(2)
Si3	−	O4	1.51(2)	WO4	−	WO4^{vii}	2.15(3)
Si3	−	O5	1.55(2)	WO1b	−	WO4b	1.61(4)
Si3	−	O4b^{iii}	1.60(2)	WO1b	−	WO3b^{viii}	2.78(5)
Si3	−	O5b^{iv}	1.62(2)	WO2b	−	WO2b	1.52(5)
N1	−	C1	1.30(2)	WO2b	−	WO4b	1.89(4)
N1	−	C2	1.59(3)	WO2b	−	O7b	2.97(2)
N1	−	C3	1.52(3)	WO3b	−	O6b^{vi}	2.14(2)
N1	−	C4	1.53(3)	WO3b	−	WO3b^{ii}	2.77(6)
				WO4	−	O7b	2.39(2)

				ϕ (°)					ϕ (°)
O2^{i}	−	Si1	− O6	110.9(3)	O5b^{iv}	−	Si3	− O5	107.8(4)
O5	−	Si1	− O3	107.8(3)	O5b^{iv}	−	Si3	− O4b^{iii}	111.3(3)
O3	−	Si1	− O2^{i}	111.0(2)	C1	−	N1	− C2	108.7(6)
O6	−	Si1	− O5	107.9(4)	C1	−	N1	− C3	109.9(3)
O1	−	Si2	− O4	108.5(4)	C1	−	N1	− C4	108.7(4)
O2	−	Si2	− O7	111.1(3)	C1	−	N1	− C5	109.9(3)
O4	−	Si2	− O2	107.5(2)	C2	−	N1	− C3	109.0(6)
O7	−	Si2	− O1	111.7(2)	C4	−	N1	− C5	109.1(4)
O2b^{ii}	−	Si1b	− O3b	110.7(7)	C2	−	N1	− C5	56.9(3)
O2b^{ii}	−	Si1b	− O6b	108.5(7)	C4	−	N1	− C3	57.0(4)
O5b	−	Si1b	− O3b	107.5(3)	C1b	−	N2	− C2b	110.2(7)
O5b	−	Si1b	− O6b	111.6(2)	C1b	−	N2	− C3b	108.8(5)
O1b	−	Si2b	− O4b	109.8(6)	C1b	−	N2	− C4b	110.1(5)
O1b	−	Si2b	− O2b	107.8(4)	C1b	−	N2	− C5b	109.1(5)
O4b	−	Si2b	− O7b	109.0(7)	C2b	−	N2	− C3b	110.6(7)
O7b	−	Si2b	− O2b	110.9(4)	C4b	−	N2	− C5b	109.9(5)
O4	−	Si3	− O5	107.9(3)	C2b	−	N2	− C5b	55.3(3)
O4	−	Si3	− O4b^{iii}	110.6(7)	C4b	−	N2	− C3b	55.0(6)

[a] Symmetry codes: (i) $x, -y + 1/2, z + 1/2$; (ii) $x, -y, z$; (iii) $-x, -y + 1/2, z - 1/2$; (iv) $-x, y, z$; (v) $x, y - 1/2, z + 1/2$; (vi) $x, -y - 1/2, z + 1/2$; (vii) $-x, -y, z$; (viii) $x, y + 1/2, z - 1/2$.

values, and only localized electron densities were visible at their locations in electron-density maps. These Q^4-type Si atoms must, hence, be ordered at the definite positions.

We finally chose the noncentrosymmetric space group *Amm*2 (no. 38), which is a maximal nonisomorphic subgroup of *Cmmm*. *Amm*2 leads to four Q^3 (8f) sites and one Q^4 site (8f), in accordance with the Q^3/Q^4 ratio obtained from the NMR spectrum (Figure 4). The x value in SiO_x, including O atoms in terminal silanol groups, is calculated to be 2.4 from the Q^3/Q^4 ratio of 4. The amount-of-substance ratio of Si/Na was then estimated at ca. 5.0 from the Si and Na contents analyzed by ICP emission spectrometry. TMA ions occupy two independent sites in space group *Amm*2.

3.2. Structure Refinement. The XRD data were analyzed by the Rietveld method with RIETAN-2000 on the ground of the above structural information. To attain stable convergence to the global minimum for the weighted sum of the squares of the residuals, we imposed constraints on parts of bond lengths and bond

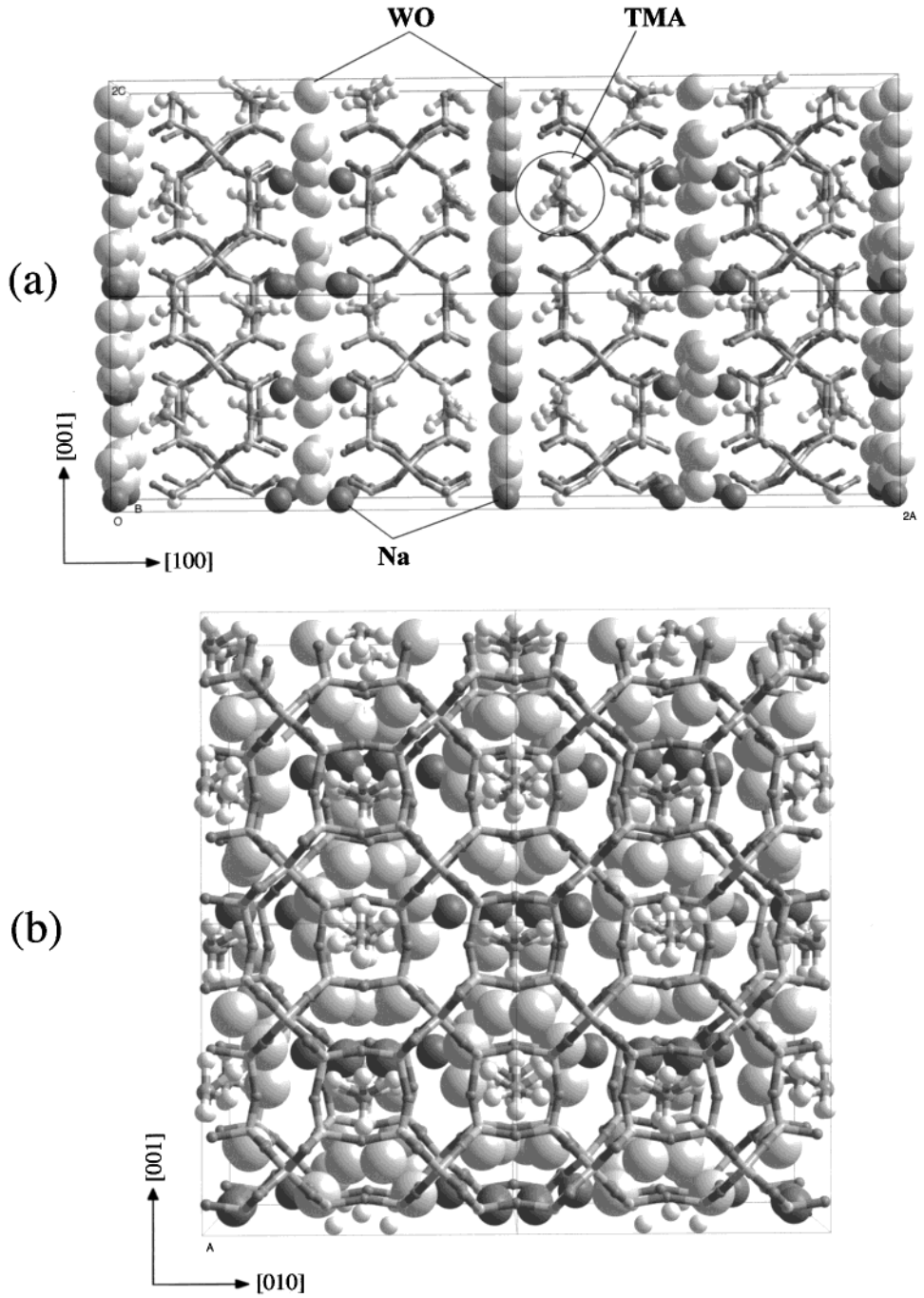

Figure 10. Perspective view of the final structural model for the HLS along the (a) [010] and (b) [010] directions. TMA ions are incorporated into cup-shaped cages.

angles, ϕ, such that l(C−N) = 1.41 ± 0.02 Å, l(Si−O) = 1.62 ± 0.05 Å, and ϕ(O−Si−O) = ϕ(C−N−C) = 109.4 ± 1.0°.

A virtual chemical species named WO, whose atomic scattering factor is equal to the sum of those for one O and two H atoms, was located in place of each H_2O molecule because the HLS contains a considerable number of H atoms. Contributions for three H atoms were similarly added to the atomic scattering factor of each C atom in a methyl group. The chemical formula of the HLS resulting from the structural model described above is $[(CH_3)_4N]_2Na_2[Si_{10}O_{20}(OH)_4]\cdot 5.5H_2O$.

From electron-density maps, we judged that three methyl groups in the TMA ion exhibit rotational disorder around a C1−N1 or a C1b−N2 bond. In other words, C atoms in the three methyl groups were split into eight sites, C2−C5 and C2b−C5b, with occupancies, g, of $^1/_2$. The remaining methyl group containing C1 or C1b is directed toward the center of the cage, in agreement with the electron-density image depicted in Figure 8. The three methyl groups containing sites C2−C5 and C2b−C5b are equivalent to each other around the 3-fold rotation axis, viz., the C1−N1 or C1b−N2 bond. Special positions (4c) were assigned to C and N sites except sites C3, C5, C3b, and C5b with fixed occupancies of g(C1) = g(C1b) = 1, g(Cn) = g(Cnb) = $^1/_2$ (n = 2−5), and g(N1) = g(N2) = 1.

Thermal motion was assumed to be isotropic for all of the sites. The following constraints were imposed on the B parameters for O sites: B(O1) = B(O2) = B(O3)

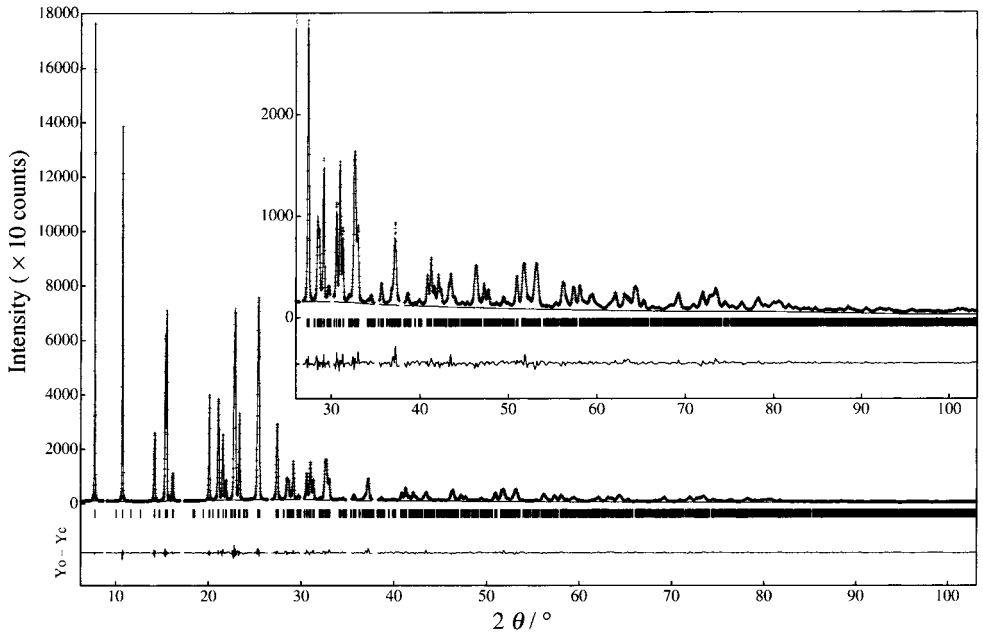

Figure 11. Rietveld refinement patterns for the HLS. The observed diffraction intensities are represented by plus (+) marks, and the calculated pattern by the solid line. Differences between observed and calculated intensities are plotted near the bottom. Short vertical marks below the observed and calculated patterns indicate the positions of allowed Bragg reflections.

$= B(\mathrm{O4}) = B(\mathrm{O5}) = B(\mathrm{O1b}) = B(\mathrm{O2b}) = B(\mathrm{O3b}) = B(\mathrm{O4b}) = B(\mathrm{O5b})$ for O sites in the frameworks and $B(\mathrm{O6}) = B(\mathrm{O7}) = B(\mathrm{O6b}) = B(\mathrm{O7b})$ for O sites in the silanol groups. Common B parameters were assigned to four groups of atoms: (1) Si, (2) Na, (3) C and N, and (4) WO. The occupancies of the WO sites were refined on the assumption that they are all equal to each other.

Table 2 lists final structure parameters of the HLS. Other crystal data are contained in Table 3. R factors were fairly low: $R_{wp} = 5.85\%$ ($R_e = 5.51\%$), $R_p = 3.86\%$, $R_B = 1.25\%$, and $R_F = 0.91\%$. Figure 10 provides a structural illustration of the HLS viewed along the (a) [100] and (b) [010] directions.

We determined final electron densities by MEM-based whole-pattern fitting using RIETAN-2000 and MEED alternately. In the whole-pattern fitting process with RIETAN-2000, structure factors were fixed at the values calculated by the MEM analysis with MEED, and the scale factor, profile, lattice, peak shift, and background parameters were refined by a least-squares method. F_o data evaluated after the whole-pattern fitting according to Rietveld's procedure[39] were analyzed again by MEM. The whole-pattern fitting and MEM analyses were alternately repeated in the above way (REMEDY cycles) until the R factors in the former no longer decrease. Such an iterative procedure is effective in minimizing the bias imposed on electron densities by the structural model adopted in the Rietveld analysis.[20,22]

A space resolution of 256 × 128 × 128 pixels per unit cell was set in the MEM analyses. After two REMEDY cycles, R factors in whole-pattern fitting decreased to $R_{wp} = 5.80\%$ ($R_e = 5.57\%$), $R_p = 3.71\%$, $R_B = 1.04\%$, and $R_F = 0.86\%$. The preceding MEM analysis of the F_o values for 1166 reflections in the region of $d > 0.97$ Å yielded R factors of $R_F = 2.54\%$ and $wR_F = 1.83\%$. The observed, calculated, and difference patterns resulting from the MEM-based whole-pattern fitting are plotted in Figure 11. Figure 12 displays an electron-density image viewed along the [010] direction.

4. Results and Discussion

As Figure 7 shows, the unique framework of the HLS contains cup-shaped cages with four- and six-membered rings. Such cages are very similar to sodalite cages divided into two pieces. Alhough all of the Si sites are fully occupied, the cup-shaped cage is locally distorted, in contrast with the cage of cubic sodalite. Calculating bond valence sums,[42] we predict l(Si−O) to be 1.62 Å for tetrahedral coordination, with an ideal bond angle of ϕ(O−Si−O) = 109.47°. The average l(Si−O) and ϕ(O−Si−O) values determined from the refined lattice and structure parameters are close to the expected values, being l(Si−O) = 1.58 Å and ϕ(O−Si−O) = 109.5°. Si−O bond lengths for the Q^3 sites vary in the wide range of 1.42−1.77 Å because bonds of O atoms attached to Q^3-type Si atoms in silanol groups are apt to be influenced by neighboring Na^+ ions and H_2O molecules. The distances between the two silicate layers vary alternately: ca. 4.0 and 4.6 Å. This fact also supports the idea that the arrangements of interlayered Na^+ ions and H_2O molecules affect the structural details of the HLS. The local distortion of the SiO_4 tetrahedra appears to be too pronounced, which can be ascribed to the limited structural information that can be extracted from our XRD data. However, structural details of the HLS is so sensitive to features of the sample environment such as humidity and temperature that the silicate layer will be readily distorted.

Electron-density images evidently reveal that the methyl groups in TMA ions encapsulated within the cup-shaped cages are rotationally disordered. In the ^{13}C MAS NMR spectrum (Figure 4), the chemical shift of the C atom in the methyl group was 57.14 ppm. This

(42) Brown, I. D.; Altermatt, D. *Acta Crystallogr.* **1985**, *B41*, 244.

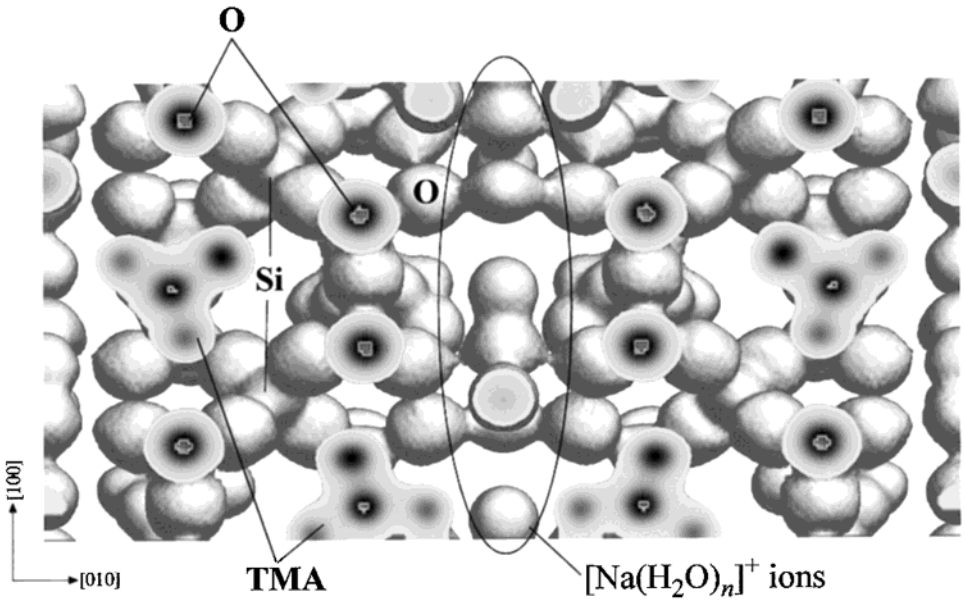

Figure 12. Electron-density image obtained after two REMEDY cycles. The orientations of methyl groups in TMA ions, Na^+ ions, and H_2O molecules are clearly seen. The equi-density level was set at 0.4 e/Å^3.

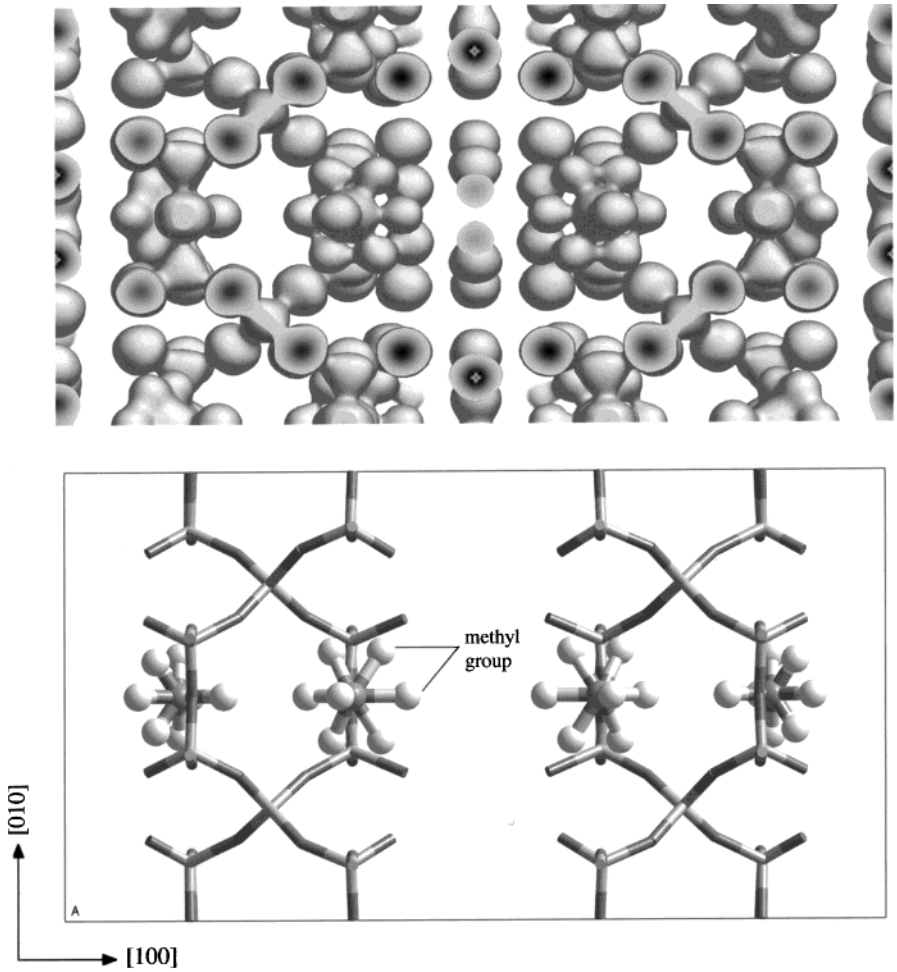

Figure 13. Electron-density image (upper) and simplified structural model (lower) viewed along the [001] direction for the z range of $0.235 \leq z \leq 1$. The rotational disorder of methyl groups is unambiguously visualized in accord with the structural model. The equi-density level was set at 0.5 e/Å^3 to facilitate a comparison.

value is larger than 56.4 ppm in RUB-15 and 56.0 ppm ion but smaller than the 58.84 ppm in sodalite,[1,43] which suggests that TMA ions in the HLS are nearer to inner frameworks in the free TMA than in RUB-15. Raman spectroscopy showed that four methyl groups arranged with T_d point-group symmetry around a N atom vibrate in the cup-shaped cages. This finding closely agrees with our structural model and the Raman spectra of other

microporous materials incorporating TMA ions.[44] As Figure 2 displays, a broad Raman band associated with variations in framework compositions appeared in the wavenumber region of 1000−1200 cm^{-1}. Bands assigned to the symmetric and asymmetric C−N stretching vibrations of the TMA ion and to the CH_3 deformation vibration were observed at 764, 958, and 1454 cm^{-1}, respectively.

Figure 13 illustrates a cutting image of electron densities in the range of $0.235 \leq z \leq 1$ and the corresponding structure drawing. Splittings of three methyl groups are unequivocally visualized. The TMA ion exhibits local rotational disorder around the 3-fold rotation axes, i.e., the C1−N1 and C1b−N2 bonds. In one TMA ion containing the C1 atom, the C1−N1 bond in one methyl group is directed toward the interior of the cage with the 3-fold rotation axis approximately parallel to the *c* axis. In the other TMA ion, the C1b−N2 bond and the *c* axis form an angle of ca. 45°. Averages of the l(C−N) and ϕ(C−N−C) values are, respectively, 1.423 Å and 109.5°, in excellent agreement with the predicted values of l(C−N) = 1.42 Å and ϕ(C−N−C) = 109.47°.

The Na^+ ions and H_2O molecules are disordered between two silicate layers in complex fashions. H_2O molecules do not surround Na^+ ions octahedrally unlike aquo ions in kanemite.[12] WO sites lie on $x = 0, {}^1/_2$ planes intermediate between the two silicate layers. The water content, ca. 5.53 per formula unit, calculated from our crystal data agrees well with that determined by TG-DTA (5.5). Site Na1 is also situated on the $x = 0$ plane, whereas site Na2 is displaced from the $x = {}^1/_2$ plane toward the TMA ion. The validity of this Na2 position needs to be examined further, but ionic linkages such as $TMA^+-OH^--Na^+$ might be locally formed with the OH^- ion bonded to a Q^3-type Si atom. The WO atoms on the $x = 0, {}^1/_2$ planes are sandwiched between the two silicate layers with different interlayer distances of ca. 4.6 Å and ca. 4.0 Å, respectively. Such a difference is explained in term of the different coordination behavior of H_2O ligands around Na^+ ions in the two kinds of the interlayer spaces.

Careful SEM observations indicate that the HLS owes its helical-stacking morphology to cleavages of larger crystals. The average thickness of crystallites perpendicular to the (100) cleavage plane was a little less than 0.5 μm, which corresponds to stacks of ca. 220 unit cells along the *a* axis. Such cleavages are most probably induced by rapid changes in the inner pressure of the autoclave and/or in the temperature. The inhomogeneity of each larger crystal might give rise to the cleavages that produce relatively uniform microcrystals.

The (100) plane tends to be twisted because the silicate layers parallel with this plane consist of $Q^3-Q^4-Q^3$ linkages and a fair number of other mobile Q^3-type Si atoms in terminal silanol groups. Such a twist will cause the cleavages that produce the helical stacking of microcrystals. Nevertheless, this framework with the cup-shaped cages is more rigid than the framework in kanemite containing only Q^3-type Si atoms. Accordingly, the HLS is expected to exhibit structural features desirable for precursors to novel high-silica microporous materials.

5. Concluding Remarks

The crystal structure of the HLS has successfully been solved by ab initio analysis using XRD data. Surprisingly, the medium-resolution intensity data measured on the conventional powder diffractometer with Cu Kα radiation provided us with enough structural information to solve such a complex structure. Electron densities determined by MEM using the partial structural models made it possible to locate TMA ions, Na^+ ions, and H_2O molecules. With MEM, we could adequately represent structural details such as chemical bonds and positional disorder, as Figures 12 and 13 demonstrate.

The framework of the HLS has a unique topology, with cup-shaped cages similar to sodalite cages split into two fractions and TMA ions incorporated into them as templates. Na^+ ions and H_2O molecules form aquo ions, $[Na(H_2O)_n]^+$ ($n \approx 4$), connecting two silicate layers to compensate for the great distortion suffered by the framework. Although some ambiguities remain regarding structural details, almost all of the atomic configurations of the framework, TMA and Na^+ ions, and H_2O molecules have been elucidated in this study. Methyl groups in the TMA ions rotate freely around the C−N bonds as they do in other cage-containing and microporous materials.

Kiyozumi et al.[45] have recently found a solid-state reaction from the HLS to TMA-containing SOD under high pressure with a very small amount of water. This reaction is believed to proceed in such a way that Na^+ ions and H_2O molecules are removed and adjacent silicate layers are connected with TMA ions encapsulated within the cage. Such a mechanism seems to be reasonable in view of our crystal data. Microporous materials derived from the cup-shaped cage can be synthesized provided that two silicate layers are cross-linked by additional Si atoms. Thus, the HLS has a bright prospect of serving as a good precursor to novel high-silica microporous materials.

Acknowledgment. We thank T. Ikeshoji of the Tohoku National Industrial Research Institute for supporting computations for part of the MEM analyses.

CM000736V

(43) Hayashi, R.; Suzuki, K.; Shin, S.; Hayamizu, K.; Yamamoto, O. *Chem. Phys. Lett.* **1985**, *113*, 368.

(44) Hong, S. B. *Microporous Mater.* **1995**, *4*, 309.

(45) Kiyozumi et al., to be submitted.